Neutron effective single-particle energies above ^{78}Ni: A hint from lifetime measurements in the $N = 51$ isotones ^{85}Se and ^{87}Kr

F. Didierjean,[1,*] D. Verney,[2] G. Duchêne,[1] J. Litzinger,[3] K. Sieja,[1] A. Dewald,[3] A. Goasduff,[1] R. Lozeva,[1,†] C. Fransen,[3] G. de Angelis,[4] S. Aydin,[5] D. Bazzacco,[5] A. Bracco,[6,7] S. Bottoni,[6,7] L. Corradi,[4] F. Crespi,[6,7] E. Ellinger,[3] E. Farnea,[4,‡] E. Fioretto,[4] S. Franchoo,[2] A. Gottardo,[4] L. Grocutt,[8] M. Hackstein,[3] F. Ibrahim,[2] K. Kolos,[2] S. Leoni,[6,7] S. Lenzi,[5] S. Lunardi,[5] R. Menegazzo,[5] D. Mengoni,[5] C. Michelagnoli,[5] T. Mijatovic,[9] V. Modamio,[4] O. Möller,[10] G. Montagnoli,[5] D. Montanari,[4] A. I. Morales,[7] D. Napoli,[4] M. Niikura,[2,§] F. Recchia,[5] E. Sahin,[4] F. Scarlassara,[5] L. Sengele,[1] S. Szilner,[9] J. F. Smith,[8] A. M. Stefanini,[4] C. Ur,[5] J. J. Valiente-Dobón,[4] and V. Vandone[6,7]

[1]*Université de Strasbourg, CNRS, IPHC UMR 7178, F-67000 Strasbourg, France*
[2]*Institut de Physique Nucléaire, CNRS/IN2P3, Univ. Paris Sud, Université Paris Saclay, F-91406 Orsay, France*
[3]*Institut für Kernphysik, Universität zu Köln, D-50937 Köln, Germany*
[4]*Instituto Nazionale di Fisica Nucleare, Laboratori Nazionali di Legnaro, I-35020 Legnaro, Italy*
[5]*Departimento di Fisica e Astronomia, Università di Padova and INFN, Sezione di Padova, I-35131 Padova, Italy*
[6]*Università degli Studi di Milano, I-20133 Milano, Italy*
[7]*INFN, Sezione di Milano, I-20133 Milano, Italy*
[8]*University of West Scotland, Praisley PA1 2EB, United Kingdom*
[9]*Ruder Boskovic Institute, HR-10000 Zagreb, Croatia*
[10]*Institut für Kernphysik, Technische Universität, D-64289 Darmstadt, Germany*

(Received 13 December 2016; revised manuscript received 20 June 2017; published 20 October 2017)

Background: While the $N = 50$ shell-gap evolution towards ^{78}Ni is presently in the focus of nuclear structure research, experimental information on the neutron effective single-particle energy sequence above the ^{78}Ni core remain scarce. Direct nucleon-exchange reactions are indeed difficult with presently available post-accelerated radioactive-ion beams (especially for high orbital-momentum orbitals) in this exotic region.
Purpose: In this study we probe the evolution of the $\nu 1g_{7/2}$ effective single-particle energy which is a key to understanding the possible evolution of the spin-orbit splitting due to the proton-neutron interaction in the ^{78}Ni region. To achieve this goal, a method based on lifetime measurements is used for the first time. The obtained lifetimes of the $7/2_1^+$ states in ^{87}Kr and ^{85}Se are used to investigate the $\nu 1g_{7/2}$ evolution.
Method: Yrast and near-yrast states in the light $N = 51$ isotones ^{85}Se and ^{87}Kr were populated via multinucleon transfer reactions, using a ^{82}Se beam and a ^{238}U target at the LNL tandem-ALPI facility. The prompt γ rays were detected by the AGATA Demonstrator and particle identification was performed using the PRISMA spectrometer. Lifetime measurements were performed by using the Cologne plunger device for deep inelastic reactions and the Recoil Distance Doppler Shift technique.
Results: We obtain $\tau_{(7/2_1^+)} = 0.4^{+1.6}_{-0.4}$ ps for ^{87}Kr. In the case of ^{85}Se an upper limit of 3(2) ps is obtained for the $\tau_{7/2_1^+}$ value.
Conclusion: For ^{87}Kr, the measured $(7/2_1^+)$ lifetime is consistent with a core-coupled $2^+ \otimes \nu 2d_{5/2}$ configuration for this state. This result is consistent with that obtained by direct reaction, which validates our method. For ^{85}Se, the measured $7/2_1^+$ lifetime limit indicates a very small contribution of the $\nu 1g_{7/2}$ configuration to the wave function of this state.

DOI: 10.1103/PhysRevC.96.044320

I. INTRODUCTION

While the $N = 50$ shell-gap evolution towards ^{78}Ni has been and continues to be the object of intense experimental investigations worldwide, attempts to experimentally determine the neutron effective single-particle energy (ESPE) sequence above the ^{78}Ni core remain scarce. This is mainly due to the fact that direct nucleon-exchange reaction experiments are extremely difficult in this hard-to-reach region, despite the considerable recent progress in radioactive-ion-beam (RIB) production techniques.

Detailed information on neutron ESPEs above $N = 50$ is available close to stability [1]; however, their evolutions towards $Z = 28$ are still poorly known or understood both from the theoretical and experimental points of view. For instance, as can be seen from Fig. 1, the general tendencies of the evolution of the ESPEs are at variance between Duflo–Zuker estimates [2] and recent shell-model calculations [3]. Precise experimental inputs to follow these evolutions are necessary and would be extremely valuable to guide the emerging shell-model developments using the ^{78}Ni natural valence space [3–8] in an effort to achieve a global, consistent description of the mass region with $Z \geqslant 28$, $N \geqslant 50$.

*francois.didierjean@iphc.cnrs.fr
†Present address: CSNSM, CNRS/IN2P3, Université Paris Sud, Université Paris Saclay, F-91405 Orsay, France.
‡Deceased.
§Present address: Department of Physics, University of Tokyo, Hongo, Bunkyo-ku, Tokyo 113-0033, Japan.

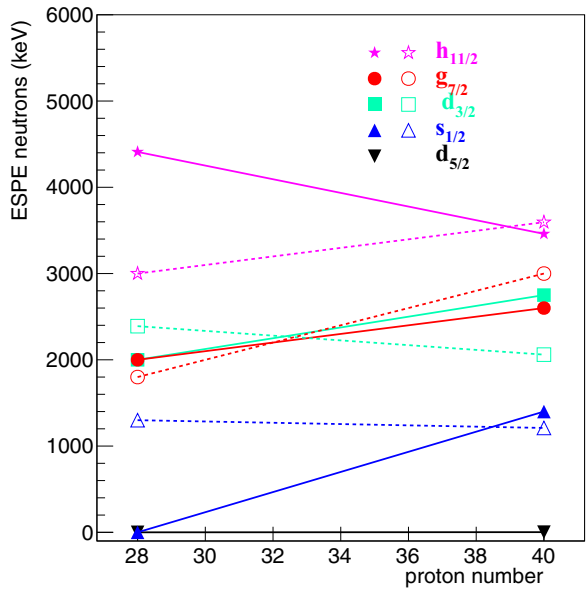

FIG. 1. Neutron single-particle energies above $N = 50$. The opened and filled symbols indicates the Duflo–Zuker estimations [2] and recent shell-model calculations [3], respectively.

On the experimental side, it is well established that the ground-state spin value of the $N = 51$ odd isotones from ^{83}Ge up to ^{101}Sn is $5/2^+$ originating from the occupation of the $\nu 2d_{5/2}$ orbital by the single valence neutron [9]. The excitation energy of the first $1/2^+_1$ excited state, which is known to carry a significant fraction of the $\nu 3s_{1/2}$ strength, is seen to decrease continuously from stability towards $Z = 32$ [10,11]. The possibility that the $\nu 3s_{1/2}$ configuration becomes the ground state at $Z = 30$, as surmised in Ref. [12] from β-delayed spectroscopy data, was thereafter ruled out [13]. A much more complete set of data is now available [14] and may allow us to answer this question. The evolution of the other neutron single-particle states in the ^{78}Ni natural valence space, $\nu 2d_{3/2}$, $\nu 1g_{7/2}$, and $\nu 1h_{11/2}$, remains an open question.

The present work aims at obtaining experimental evidence on the evolution of the $\nu 1g_{7/2}$ ESPE. Since this state is characterized by a high orbital angular momentum ℓ, one expects this evolution to be dominated by a strong tensor proton-neutron interaction term. Indeed, the rapid $\nu 1g_{7/2}$ ($\ell_\downarrow$) ESPE drop, from $Z = 40$ to $Z = 50$, as the proton $\pi 1g_{9/2}$ ($\ell_\uparrow$) shell is being filled, is a salient feature of the heaviest $N = 51$ isotones (see Ref. [9] and references therein) which almost leads to a $\nu 2d_{5/2}$-$\nu 1g_{7/2}$ degeneracy in the ^{100}Sn region. This phenomenon is one of the earliest examples used by Otsuka *et al.* to illustrate the importance of tensor terms in explaining shell evolutions far from stability [15,16]. One of the robust features of this tensor mechanism is that strong attractive proton-neutron $\pi(\nu)\ell_\downarrow$-$\nu(\pi)\ell_\uparrow$ terms are necessarily associated with repulsive $\pi\ell_\uparrow$-$\nu\ell_\uparrow$ or $\pi\ell_\downarrow$-$\nu\ell_\downarrow$ ones. In that perspective, the $\nu 1g_{7/2}$ ($\ell_\downarrow$) should be less and less bound as the proton $\pi 1f_{5/2}$ ($\ell_\downarrow$) orbital is being filled just after the $Z = 28$ shell closure. On the contrary, the binding energy of the $\nu 2d_{5/2}$ ($\ell_\uparrow$) orbital should increase, thus leading to an increasingly large energy gap between $\nu 2d_{5/2}$ and $\nu 1g_{7/2}$ orbitals. A robust prediction resulting from this mechanism should be the observation at lower and lower energies of states, having sizable $\nu 1g_{7/2}$ components, in the $N = 51$ isotones starting from stability towards ^{79}Ni.

Considering now the neutron transfer data, for ^{87}Kr (populated from the lightest stable $N = 50$ target available) the main component with $\ell = 4$ is found for the $7/2^+_2$ state located near 2.52 MeV excitation energy [1,17] with a large spectroscopic factor $S = 0.49$ [17] while the $7/2^+_1$ state carries no strength. The situation is much less clear in the case of ^{85}Se which was populated in the ^{2}H(^{84}Se,p)^{85}Se reaction [11]: the $7/2^+_1$ located at 1115 keV was weakly populated in the reaction but the small observed cross section appeared to be compatible with $\ell = 4$ associated with a large spectroscopic factor $S = 0.77 \pm 0.27$. This would mean that the $\nu 1g_{7/2}$ single-particle energy undergoes a sudden and huge decrease of more than 1 MeV from ^{87}Kr to ^{85}Se. However, the statistics obtained in this experiment was too low to exclude a $\ell = 2$ configuration for this state [11] (there is no obvious reason to question the $J^\pi = 7/2^+$ assignment made to this state, which was systematically populated in deep-inelastic [18], fusion-fission [19], and beta-decay [20,21] experiments). While direct nucleon-exchange studies will remain impeded for a while due to low available RIB intensities and, more importantly, for high-ℓ orbits, with unsatisfactory matching conditions due to available RIB energies, we propose with this work an alternative method suitable for the specific case of the $\nu 1g_{7/2}$ orbital in this region, based on lifetime measurements.

Our method relies on the basic idea that, next to the $N = 50$ shell closure, the mixing of the only two main possible core-coupled configurations, $2^+ \otimes \nu 2d_{5/2}$ and $0^+ \otimes \nu 1g_{7/2}$ in the $7/2^+_1$ state, should dominate the $7/2^+_1 \rightarrow 5/2^+_{gs}$ transition properties i.e. the $7/2^+_1$ lifetime, $\tau_{7/2^+_1}$. Since, based on systematics, it is reasonable to assume $0^+ \otimes \nu 2d_{5/2}$ as the main configuration in the $5/2^+_{gs}$ state, this transition should lie between two extreme situations: a core ("collective" in a sense) $2^+ \otimes \nu 2d_{5/2} \rightarrow 0^+ \otimes \nu 2d_{5/2}$ transition, or a much slower single-particle one $0^+ \otimes \nu 1g_{7/2} \rightarrow 0^+ \otimes \nu 2d_{5/2}$. A relative increase of the $\nu 1g_{7/2}$ component in the ^{85}Se $7/2^+_1$ state should in principle be evidenced by comparing its lifetime with the one of the $7/2^+_1$ state of ^{87}Kr, its $N = 51$ odd neighbor, which is clearly nonstripped in direct reactions (i.e., negligible $\nu 1g_{7/2}$ component).

To achieve this goal, yrast and near-yrast states were populated in the light $N = 51$ isotones ^{85}Se and ^{87}Kr via multinucleon transfer reactions by using a ^{82}Se beam and a ^{238}U target at the Laboratori Nazionali di Legnaro (LNL) tandem Acceleratore Lineare Per Ioni (tandem-ALPI) facility. Prompt γ rays were detected by the Advanced Gamma Tracking Array (AGATA) Demonstrator and particle identification was achieved by using the PRISMA spectrometer. Lifetime measurements were performed by using the Cologne plunger device for deep inelastic reactions and the Recoil Distance Doppler Shift technique. After giving some details on the experiment (Sec. II) and the lifetime extraction (Sec. III) procedures, we report in Sec. IV on the results of our lifetime measurements. For ^{87}Kr, intrinsic lifetimes of seven states including the $(7/2^+_1)$ and $9/2^+_1$ states could be determined

for the first time. These values were obtained within various assumptions on the nature of the unobserved feeding of these states. In the case of ^{85}Se, where the statistics was significantly lower, two effective lifetimes could be determined for the transitions from the $7/2_1^+$ and $(9/2_1^+)$ states to the ground state. They are proposed as upper limits for the real lifetimes of these two states. Finally, the results concerning the $7/2_1^+$ states in ^{87}Kr and ^{85}Se are discussed in Sec. V by using two different approaches a schematic core-coupling model and a fully microscopic shell model. The former approach is used as a toy model to extract an upper limit for the $\nu 1g_{7/2}$ component in the ^{85}Se $7/2_1^+$ state.

II. EXPERIMENT

The experiment was performed at the LNL tandem-ALPI accelerator complex. The ^{87}Kr and ^{85}Se nuclei were produced by multinucleon transfer reactions induced by a ^{82}Se beam, impinging with an energy of 577 MeV on a ^{238}U target. The latter with a thickness of 2 mg/cm^2 was evaporated onto a 1.2 mg/cm^2 Ta backing which was facing the beam and was rotated by an angle of 43° relative to the beam direction. The beam energy at the center of the ^{238}U target was about 530 MeV and the average beam intensity was 1.2 pnA.

The projectile-like nuclei were identified and their velocities were determined with the magnetic spectrometer PRISMA [22,23] located at the grazing angle of 58°. The unambiguous identification of the reaction products in PRISMA is based on the ion-trajectory reconstruction using (i) the x and y entrance coordinates on the microchannel plate (MCP), (ii) the x and y coordinates on the array of parallel plates of the multiwire chambers (MWPPAC) located at the focal plane, (iii) the projectile-like residue time of flight (TOF) between the MCP and the MWPPAC, (iv) the partial (ΔE) and total energies (E) released in the ionization chamber (IC) which is composed of 40 sections. The selection of the atomic number (Z) was made by using two complementary correlation matrices: (i) the energy loss (ΔE) in the first row of 10 IC sections versus E and (ii) E versus the range of the ion in IC (see Fig. 1 in Ref. [22]). The isotope selection was performed in two steps. First, the ion charge state (q) is identified in a bidimensional matrix E versus $r \cdot \beta$, where r is the curvature radius of the ion trajectory in the PRISMA dipole. For each charge state, the mass distribution was obtained, enabling the selection of PRISMA events of a given mass A (Fig. 2).

The prompt γ rays were detected by the AGATA Demonstrator [24,25]. The setup comprised five triple cluster modules placed at 18.6 cm to the target and at backward angles between 143° and 174°. By using the grid search algorithm [26] for pulse shape analysis (PSA), the γ-ray interaction points were located in the Ge material with a resolution of about 5 mm at 1 MeV [27,28]. The energies of γ rays were obtained by applying offline the Orsay Forward Tracking (OFT) γ-ray tracking algorithm [29]. The γ-ray spectrum of the nuclei of interest is Doppler corrected event by event by using the velocity vector measured in PRISMA and the position of the first interaction in AGATA.

Lifetime measurements were performed by using the recoil distance Doppler shift (RDDS) technique using the Cologne plunger device for deep inelastic reactions [30,31]. A ^{93}Nb degrader foil with a thickness of 4.15 mg/cm^2 was placed downstream of the target to slow down the projectile-like residues. Depending on the lifetime of the state of interest and the distance between target and degrader, γ-ray emission may happen partially before and after the degrader at respective recoil velocities β_{before} and β_{after}. Consequently, for each transition, two peaks "before" and "after" are observed in the γ-ray spectrum. Because β_{after} is precisely calculated from PRISMA information, the "after" component is accurately Doppler corrected (unshifted peak) whereas the "before" component is shifted to lower energy (AGATA being placed at backward angles). Lifetimes are deduced from the ratio of intensity of the two components. The degrader was placed at two distances from the target [32]: 38(1) μm and 257(2) μm with a measuring time of 30 and 80 h, respectively.

^{87}Kr spectra are shown in Fig. 3. The intensities of the shifted and unshifted peaks are extracted from a background-subtracted spectrum by using a normalized fraction of all PRISMA data except for Se (red curve in Fig. 3).

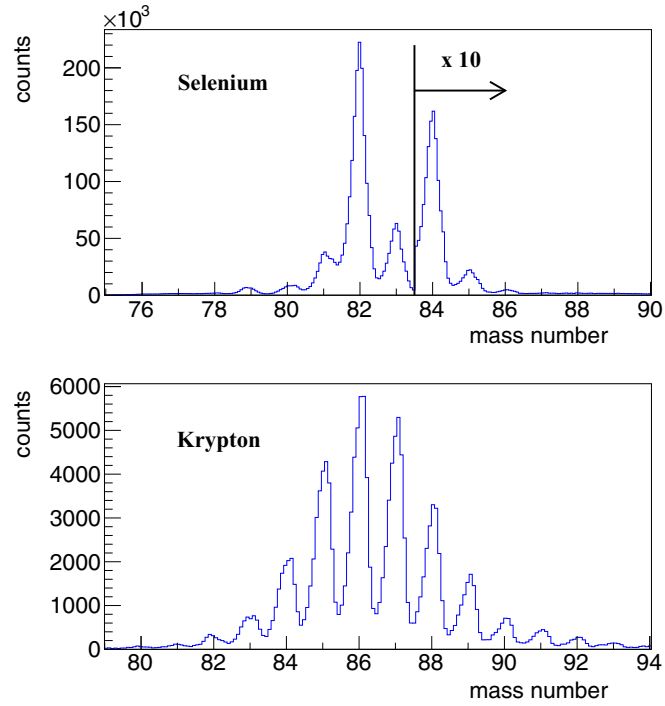

FIG. 2. Mass spectra of Se (top) and Kr (bottom) isotopes for a charge state of $q = 25^+$.

III. ANALYSIS PROCEDURE

The effective lifetime τ_i^{eff}, which describes the cumulative lifetime of a given excited state i including all feeding times from the cascades of levels above that level, is expressed as a function of the target-to-degrader distance d and the intensity ratio R_i as

$$\tau_i^{\text{eff}} = -\frac{d}{v \ln(R_i)}, \quad (1)$$

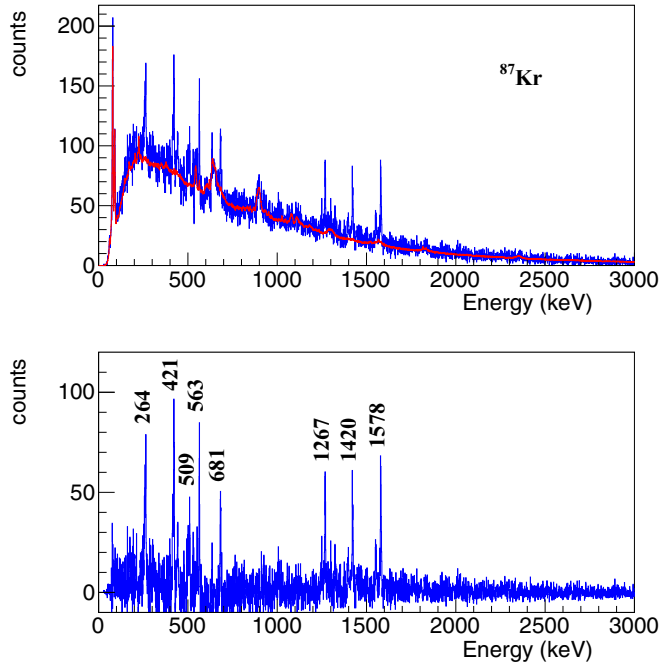

FIG. 3. (top panel) γ-ray spectrum in coincidence with ^{87}Kr ions identified in PRISMA (blue histogram). The red curve corresponds to the γ spectrum in coincidence with all nuclei except for Se ions identified in PRISMA. (bottom panel) ^{87}Kr background-subtracted γ-ray spectrum.

with

$$R_i = \frac{I_{\text{after}}}{I_{\text{before}} + I_{\text{after}}}, \tag{2}$$

where R_i is related to the shifted (I_{before}) and the unshifted (I_{after}) components of the transition i as observed in the γ-ray spectra.

The velocity between the target and the degrader, v in Eq. (1), is calculated by using the LISE++ program [33] from the mean β values of the ions after the degrader measured in PRISMA. Velocities before and after degrader are around 9% and 7% of light velocity, respectively, for both ^{87}Kr and ^{85}Se nuclei.

The effective lifetime of a given level, obtained from the experimental data by using Eq. (1), includes besides the intrinsic lifetime of the level to be determined the complete history, i.e., the (complex) time behavior of all the observed and unobserved feeding transitions. Due to limited available target-to-degrader distances in our experiment, standard RDDS analysis techniques [34] cannot be exploited and we have chosen a suitable variant based on direct resolution of the Bateman equation system as follows. We assume the situation illustrated in Fig. 4 where the state of interest k, with a decay constant λ_k, is fed directly by an observed transition depopulating a state $k-1$, with a decay constant λ_{k-1}, and by a set of unobserved side-feeding transitions which are taken into account by assuming a single transition deexciting a virtual state sf with a decay constant $\lambda^{\text{sf}}_{k-1}$. Assuming this simplified

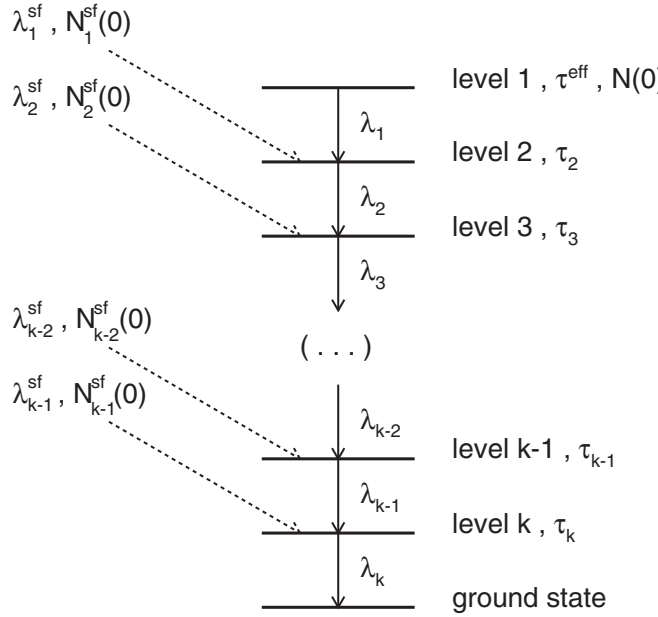

FIG. 4. Simplified decay network as assumed in the lifetime extraction procedure.

decay network, the evolution of the population of states k as function of time, $N_k(t)$, is related to the evolutions of the populations of states $k-1$, $N_{k-1}(t)$, and sf, $N^{\text{sf}}_{k-1}(t)$ by

$$\frac{dN_k(t)}{dt} = \lambda_{k-1}N_{k-1}(t) - \lambda_k N_k(t) + \lambda^{\text{sf}}_{k-1}N^{\text{sf}}_{k-1}(t). \tag{3}$$

The resolution of Eq. (3) gives

$$N_k(t) = N(0)\left(\prod_{\ell=1}^{k-1}\lambda_\ell\right)\sum_{i=1}^{k}\frac{e^{-\lambda_i t}}{\prod_{\substack{j=1\\ i\neq j}}^{k}(\lambda_j-\lambda_i)} + \sum_{n=1}^{k-1}\left[N_n^{sf}(0)\left(\prod_{\ell=n}^{k-1}\lambda_\ell^{(n)}\right)\sum_{i=1}^{k}\frac{e^{-\lambda_i^{(n)}t}}{\prod_{\substack{j=n\\ i\neq j}}^{k}\left(\lambda_j^{(n)}-\lambda_i^{(n)}\right)}\right], \tag{4}$$

where the level numbering follows the notation introduced in Fig. 4. For each level k, the side feeding to all upper levels $n \leqslant k-1$ is taken into account by the second term of this equation, where the compact notation $\lambda^{(n)}_{\ell,i,j}$ stands for $\lambda^{(n)}_\ell = (\lambda^{\text{sf}}_n, \lambda_{n+1}, \ldots, \lambda_{k-1})$ and $\lambda^{(n)}_{i,j} = (\lambda^{\text{sf}}_n, \lambda_{n+1}, \ldots, \lambda_k)$ (i.e., the intrinsic decay constant λ_p, where p equals ℓ, i, or j, is replaced by the decay constant λ^{sf}_n of the side feeding to level n when $p = n$). The number of emitted γ rays between the target and the degrader is obtained by integration of Eq. (4)

which reads

$$\xi = \lambda_i \int_0^t N_k(t)dt = N(0)\left(\prod_{\ell=1}^{k}\lambda_\ell\right)\sum_{i=1}^{k}\frac{1-e^{-\lambda_i t}}{\lambda_i\prod_{\substack{j=1\\ i\neq j}}^{k}(\lambda_j-\lambda_i)} + \sum_{n=1}^{k-1}\left[N_n^{sf}(0)\left(\prod_{\ell=n}^{k}\lambda_\ell^{(n)}\right)\sum_{i=n}^{k}\frac{1-e^{-\lambda_i^{(n)}t}}{\lambda_i^{(n)}\prod_{\substack{j=n\\ i\neq j}}^{k}\left(\lambda_j^{(n)}-\lambda_i^{(n)}\right)}\right], \quad (5)$$

where t represents the time of flight of the ion for the target-to-degrader distance d with $v_{\text{before}} = d/t$. The ratio R_k is calculated as follows:

$$R_k = 1 - \frac{\xi}{N(0) + \sum_{n=1}^{k-1} N_n^{\text{sf}}(0)}. \quad (6)$$

Thus, the lifetime of the level of interest can be graphically estimated by applying the following procedure: (i) the effective lifetime (τ_1^{eff}) of state 1 is calculated by using Eq. (1) and λ_1 is deduced ($\lambda_1 = 1/\tau_1^{\text{eff}}$), (ii) λ_1 and λ_1^{sf} are used in Eq. (6), λ^{sf} being chosen following different hypotheses on the side-feeding lifetime (see Sec. IV), and (iii) $R_2(\tau_2)$ can then be numerically expressed from Eq. (6) as a continuous and increasing function of τ_2. Its crossing point with the measured R_2^{expt} value determines the lifetime value for a given state 2, τ_2 (as shown in Fig. 5). The same procedure is iterated to determine the lifetimes of the different levels i going down along the γ-ray cascade.

IV. LIFETIME RESULTS

A. Lifetime measurements of excited states in ^{87}Kr

For the short plunger distance (38 μm), the statistics for low intensity γ rays was insufficient to extract the effective lifetimes. For the two intense peaks, corresponding to 1420 and 1578 keV in Fig. 6, the intensity ratio, calculated with Eq. (2), is around 0.9. However, in this range, a small variation of the R value leads to a large uncertainty of the lifetime determination, as shown in Fig. 7. Thus, in the following, the effective lifetime values are obtained by using only the measurements taken at 257 μm plunger distance (light red region in Fig. 7).

Figure 8 shows the spectrum region centered around the energies of the two most intense transitions $(7/2_1^+) \rightarrow 5/2_{\text{gs}}^+$ and $9/2_1^+ \rightarrow 5/2_{\text{gs}}^+$ (at 1420 and 1578 keV, respectively) along with those of the two main transitions feeding the $(7/2_1^+)$ and $9/2_1^+$ states (at 421 and 681 keV, respectively). The shifted-to-unshifted intensity ratios R, as given by Eq. (2), were obtained from a Gaussian fit of the experimental data by using the chi-square minimization routine in ROOT [35], shown by the continuous red curves in Fig. 8. In the fit procedure, the width and energy centroid of the peaks were fixed at the values extracted from spectra containing the full statistics of the experiment.

B using the method described in Sec. III, we extracted the intrinsic lifetimes of most of the states represented in Fig. 9, starting from effective lifetimes of the highest-lying states for which R_i could be determined within our statistics; see Table I. Uncertainties on R_i, with $i < k$, were strictly propagated to the lifetime determination for each level k. The side feeding to each state was determined from the observed feeding and deexciting γ-intensity balance.

Two assumptions for the side-feeding lifetime were made: (i) a long-lived side-feeding value of $\tau_{\text{sf}} = 17(1)$ ps (corresponding to the mean of the seven effective lifetimes of states below the 563 keV transition) and (ii) a short-lived side feeding $\tau_{\text{sf}} = 0.001$ ps in the assumption of direct (instantaneous) feeding by the reaction. This leads to the lifetime values reported in Table I.

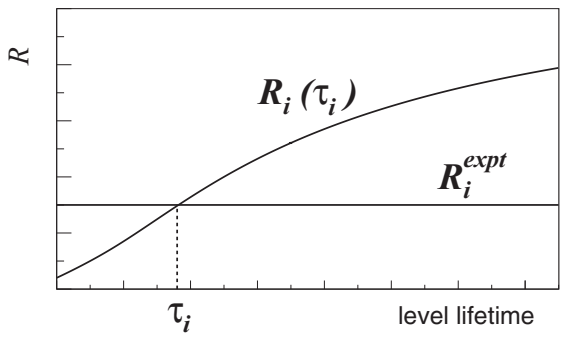

FIG. 5. Schematic $R(\tau)$ curve that allows us to determine the level lifetime τ_i.

B. Lifetime measurements of excited states in ^{85}Se

In Fig. 10 are shown the γ-ray spectra for ^{85}Se events, centered at the energy of the $7/2_1^+ \rightarrow 5/2_{\text{gs}}^+$ and $(9/2_1^+) \rightarrow 5/2_{\text{gs}}^+$ transitions (at 1115 and 1436 keV, respectively) for the two target-to-degrader distances (38 and 257 μm). Due to poor statistics, no other transition could be exploited from the spectra. The resulting rudimentary level scheme of ^{85}Se is given in Fig. 11 based on transition placements from

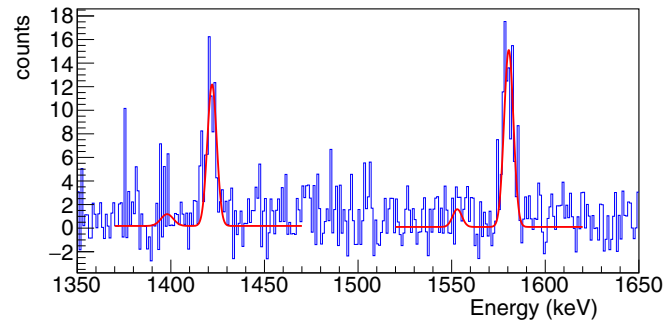

FIG. 6. γ-ray spectrum of ^{87}Kr after background subtraction for a target-to-degrader distance of 38 μm. The red curves correspond to Gaussian fits of the shifted and unshifted components of the $(7/2_1^+) \rightarrow 5/2_{\text{gs}}^+$ and $9/2_1^+ \rightarrow 5/2_{\text{gs}}^+$ transitions at 1420 and 1578 keV, respectively.

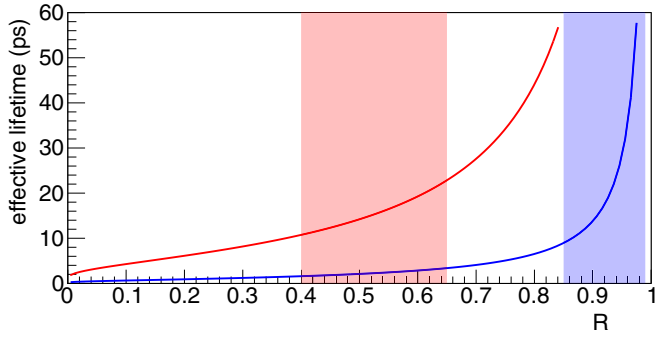

FIG. 7. Variation of the effective lifetimes calculated from Eq. (1) as a function of the intensity ratio R. The blue and red curves correspond to the plunger distances of 38 and 257 μm, respectively. The light blue and light red areas show the range of R values observed in this work for transitions in ^{87}Kr at 38 and 257 μm, respectively.

Refs. [18,19,21]. The R values and the effective lifetimes obtained by using Eqs. (1) and (2) are listed in Table II. Because no information on the direct feeding of the $7/2^+_1$ and $(9/2^+_1)$ states has been previously reported [18,19], we can only propose an upper lifetime limit of 3(2) ps for both states $7/2^+_1$ and $(9/2^+_1)$.

C. Adopted lifetime values of $7/2^+_1$ and $9/2^+_1$ states in ^{85}Se and ^{87}Kr

In conclusion, in view of the forthcoming discussion, we adopt for the $(7/2^+_1)$ and $9/2^+_1$ excited states in ^{87}Kr

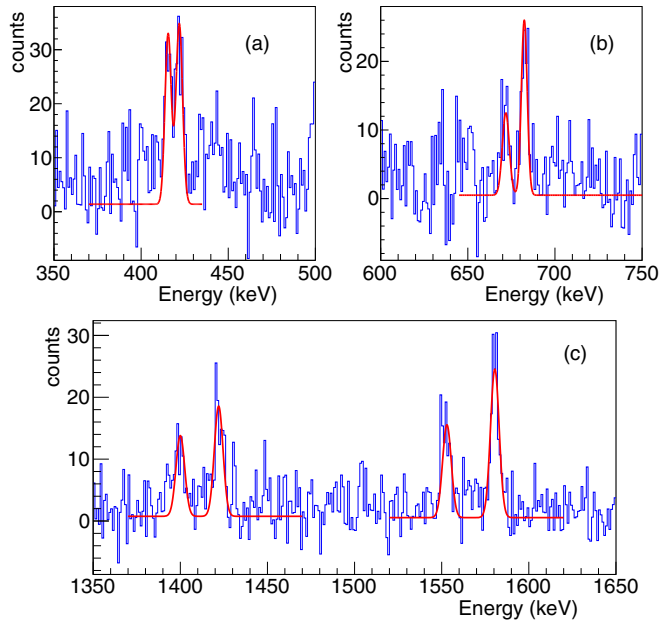

FIG. 8. γ-ray spectrum of ^{87}Kr after background subtraction for a target-to-degrader distance of 257 μm. The red curves correspond to Gaussian fits of the shifted and unshifted components of the (a) $(9/2^+_2) \rightarrow (7/2^+_1)$ transition at 422 keV, (b) $11/2^-_1 \rightarrow 9/2^+_1$ transition at 681 keV, and the (c) $(7/2^+_1) \rightarrow 5/2^+_{gs}$ and $9/2^+_1 \rightarrow 5/2^+_{gs}$ transitions at 1420 and 1578 keV, respectively.

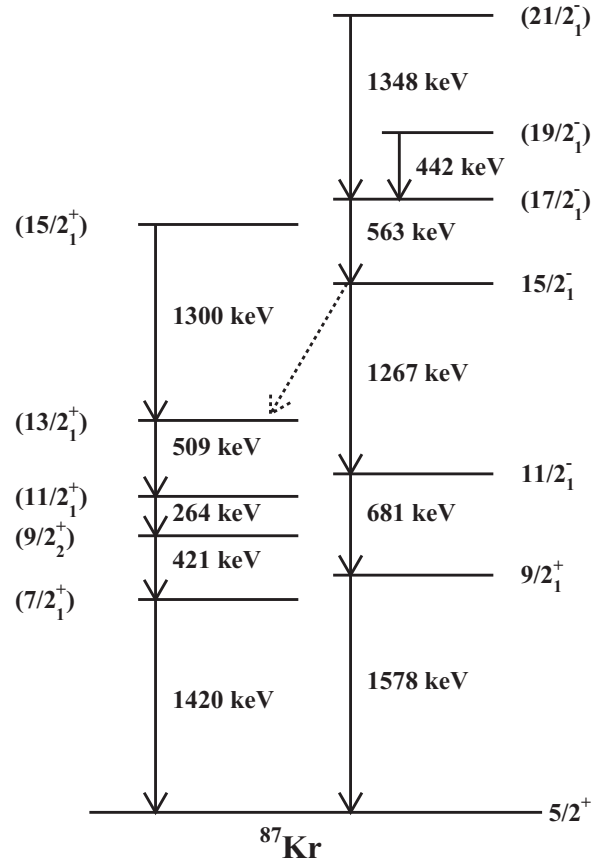

FIG. 9. Level scheme of ^{87}Kr as observed in the present work. Because the statistics was insufficient to obtain coincidence relationships, the spin assignments are from Ref. [36]. The dotted arrow represents the not-exploitable 911 keV transition.

the lifetimes $\tau_{(7/2^+_1)} = 0.4^{+1.6}_{-0.4}$ ps and $\tau_{9/2^+_1} \leqslant 0.1$ ps, which were obtained by using the empirical assumption that the unobserved feeding time is equal to the average of the observed effective lifetimes. This is not only a standard assumption [31] in similar situations but is also the most probable hypothesis in our specific case. Concerning ^{85}Se there is not much choice but to keep the upper values reported in Table II.

V. DISCUSSION

A systematics of some of the excitation levels of interest for the light $N = 51$ odd isotones is given in Fig. 12 for the sake of clarity. The coupling of the single neutron in the $\nu 2d_{5/2}$ orbital to the $N = 50$ core 2^+ excitation leads to a multiplet of five states from $1/2^+$ to $9/2^+$. Its excitation-energy center of gravity is about the one of the core 2^+ excitation energy with, in the case of quadrupole core excitation, the $7/2^+$ state as the lowest-lying multiplet member [37]. As can be seen in Fig. 12, the observed excitation energy of the $9/2^+_1$ states follows closely those of the $N = 50$ core 2^+ states, showing their core-coupled nature [9] for the isotones considered here. As explained in Sec. I, large spectroscopic factors were measured for the $1/2^+_1$ states, indicating a large contribution of the $\nu 3s_{1/2}$ orbital. Therefore, it is not expected

TABLE I. Effective lifetimes $\tau^{\rm eff}$ and intrinsic lifetimes τ of excited levels in ^{87}Kr obtained in the present experiment with two different assumptions for the side-feeding lifetime. The spin and parity of each state, its depopulating transition energy E_γ, and relative intensity I_γ calculated versus the sum of 1420 and 1578 keV transitions intensities are given. R represents the intensity ratio [Eq. (2)] for the target-to-degrader distance $d = 257$ μm. States with τ values marked by * have no side feeding according to the observed gamma-intensity balance.

Excited state, J^π	E_γ (keV)	I_γ (%)	R	$\tau^{\rm eff}$ (ps)	τ (ps) Long-lived side feeding	τ (ps) Short-lived side feeding
$(7/2_1^+)$	1420	45(3)	0.55(4)		$0.4^{+1.6}_{-0.4}$	$3.5^{+1.6}_{-1.4}$
$(9/2_2^+)$	421	36(4)	0.53(4)		$0.3^{+1.6}_{-0.3}$	$6.0^{+1.6}_{-1.6}$
$(11/2_1^+)$	264	22(4)	0.49(5)		$1.8^{+1.0}_{-1.0}$ *	$1.8^{+1.0}_{-1.0}$ *
$(13/2_1^+)$	509	25(3)	0.41(5)	11(3)		
$9/2_1^+$	1578	55(3)	0.61(4)		$\leqslant 0.1$	$5.0^{+1.8}_{-5.0}$
$11/2_1^-$	681	33(3)	0.64(5)		$0.1^{+1.5}_{-0.1}$	$\leqslant 2.1$
$15/2_1^-$	1267	33(3)	0.62(5)		$\leqslant 1.0$	$0.6^{+1.4}_{-0.6}$
$(17/2_1^-)$	563	31(3)	0.72(8)		$23.1^{+11.3}_{-6.3}$ *	$23.1^{+11.3}_{-6.3}$ *
$(19/2_1^-)$	442	5(3)	0.58(7)	18(6)		
$(21/2_1^-)$	1348	30(5)	$\leqslant 0.11$	$\leqslant 4$		

that they belong to the core-coupled multiplet although some mixing with its $1/2_2^+$ member cannot be excluded. The $7/2_1^+$ states for $Z = 36$–42 with small spectroscopic factors [1] (open red circles in Fig. 12) are dominated by the core-coupled configuration, whereas the $7/2_2^+$ states are more likely of single-particle nature (full red circles in Fig. 12). Assuming that the nature of the $7/2_1^+$ state in ^{85}Se is of $\nu 1g_{7/2}$ character as suggested in Ref. [11], one would obtain a sudden and huge decrease of its ESPE of more than 1 MeV from ^{87}Kr to ^{85}Se.

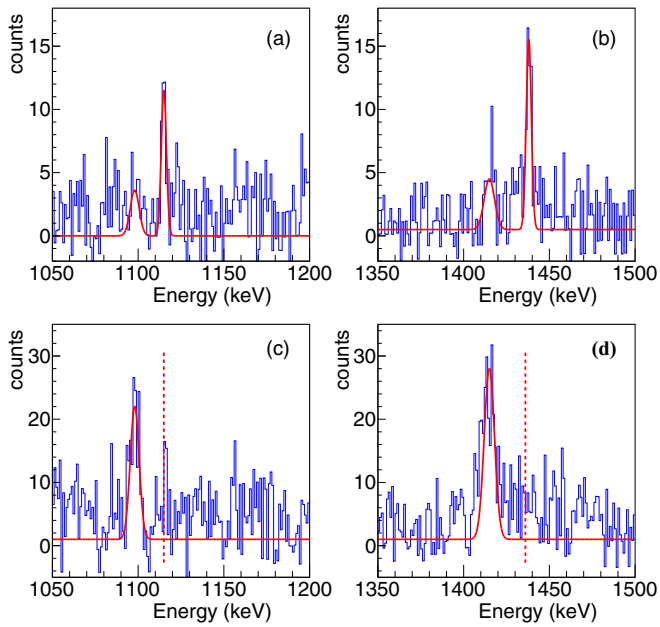

FIG. 10. Background-subtracted γ-ray spectra of ^{85}Se for the target-to-degrader distances of (a), (b) 38 μm and (c), (d) 257 μm. The red curves correspond to Gaussian fits of the shifted and unshifted components of (a), (c) the $7/2_1^+ \rightarrow 5/2_{\rm gs}^+$ and (b), (d) $(9/2_1^+) \rightarrow 5/2_{\rm gs}^+$ transitions at 1115 and 1436 keV, respectively. The dashed lines [panels (c) and (d)] show the location of the unshifted peak for the plunger distance of 257 μm.

In the following section we propose a description of the $N = 51$ odd isotones making full use of the apparent core-coupling nature of their structure. The lifetime results of these calculations will then be compared with those obtained by a fully microscopic treatment within the shell model.

A. Core-coupling approach

Calculations were performed following a procedure similar to the one already described in Ref. [38] and in references therein. In the present case, we restrict these calculations only to odd systems. In particular, our calculations should be seen as an attempt to verify whether the results obtained by Hoffmann–Pinther and Adams for the ^{89}Sr case [39] can be extended to lighter $N = 51$ isotones ^{87}Kr and ^{85}Se. We recall here only some of the calculation ingredients which are the most relevant for the present discussion.

Within the core-coupling approach, the form of the Hamiltonian describing the $N = 51$ odd-systems is

$$H = H_c + H_n + H_{\rm int},$$

where H_c and H_n are the Hamiltonians of the $N = 50$ even-even core and the odd-neutron single particle, respectively. $H_{\rm int}$ is the interaction between the core and the particle for which we use the schematic version of Thankappan and

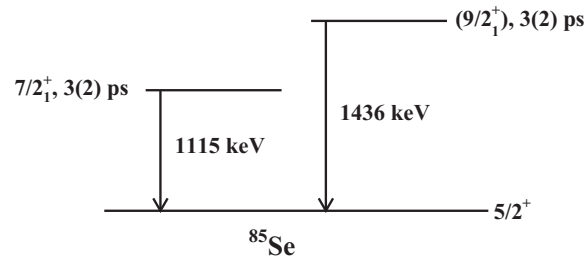

FIG. 11. Effective lifetimes for the $7/2_1^+$ and $(9/2_1^+)$ states in ^{85}Se observed in this work. The level placement is from Refs. [18,19,21].

TABLE II. Effective lifetimes of transitions in ^{85}Se. R represents the intensity ratio [Eq. (2)] for the two target-to-degrader distances.

Transition	E_γ (keV)	$d(\mu$m)	R	τ^{eff} (ps)
$7/2_1^+ \rightarrow 5/2_{\text{gs}}^+$	1115	38	0.65(3)	3(2)
		257	$\leqslant$0.11	$\leqslant$4
$(9/2_1^+) \rightarrow 5/2_{\text{gs}}^+$	1436	38	0.65(3)	3(2)
		257	$\leqslant$0.11	$\leqslant$4

True [40]:

$$H_{\text{int}} = -\xi \mathbf{J}_c^{(1)} \cdot \mathbf{j}_n^{(1)} - \eta \mathbf{Q}_c^{(2)} \cdot \mathbf{Q}_n^{(2)},$$

where $\mathbf{J}_c^{(1)}$ and $\mathbf{j}_n^{(1)}$ correspond to the angular-momentum operators of the core and the neutron single particle, and $\mathbf{Q}_{c,n}^{(2)}$ are the mass quadrupole operators for the core and the neutron single particle. The Hamiltonian is diagonalized in the basis of vectors $|J_c, j_n; JM\rangle$ which are eigenfunctions of $H_c + H_n$. The total angular-momentum operator of the system is $\mathbf{J}^{(1)} = \mathbf{J}_c^{(1)} + \mathbf{j}_n^{(1)}$, and its z-component quantum number is denoted M. The neutron is allowed to occupy the set of positive-parity single-particle states $\{2d_{5/2}; 3s_{1/2}; 2d_{3/2}; 1g_{7/2}\}$. The core states are restricted to the 0_{gs}^+ and 2_1^+ states to keep a reasonable number of core-coupling strength parameters since no assumption is (voluntarily) made on the nature of the core dynamics. The core 2_1^+ excitation energy is taken from the experiment and the

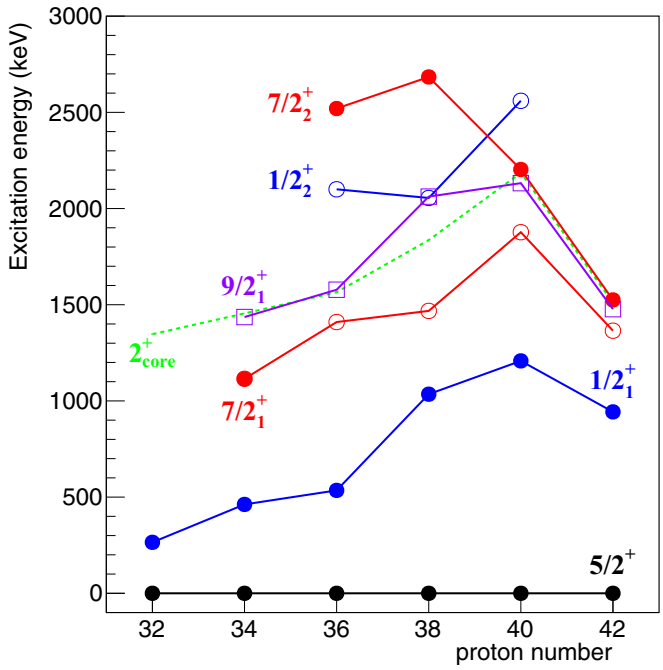

FIG. 12. Systematics of some of the states of interest for the present discussion, for the light $N = 51$ odd isotones from $Z = 32$ to 42 (adapted from Ref. [9]). The evolution of the 2^+ core-excited state in $N = 50$ nuclei is also shown (green line). The $5/2^+$ ground states are shown in black, the $1/2^+$ and the $7/2^+$ states in blue and in red, respectively. The filled (open) circle symbols indicate the large (small) spectroscopic factors. The first $9/2^+$ states are shown with purple square symbols.

TABLE III. Experimental [41,44] and calculated ground-state static magnetic-dipole μ and electric-quadrupole Q moments for ^{89}Sr, ^{87}Kr, and ^{85}Se. Subscripts "CC," "expt" and "SM" indicate core-coupling model, experimental, and shell-model values, respectively.

	μ_{CC} (n.m.)	μ_{expt} (n.m.)	μ_{SM} (n.m.)	Q_{CC} (eb)	Q_{expt} (eb)	Q_{SM} (eb)
^{89}Sr	-1.020	$-1.1481(8)$	-1.196	-0.27	$-0.271(9)$	-0.25
^{87}Kr	-1.042	$-1.023(2)$	-1.201	-0.26	$-0.30(3)$	-0.27
^{85}Se	-1.048		-1.180	-0.28		-0.28

core-coupling strength parameters are adjusted to reproduce the experimental positive-parity level-scheme patterns. In these conditions following the Thankappan–True approach, it is convenient to parametrize the quadrupole strength under the form

$$\chi_1 = \eta \langle 0^+ \| \mathbf{Q}_c^{(2)} \| 2^+ \rangle,$$
$$\chi_2 = \eta \langle 2^+ \| \mathbf{Q}_c^{(2)} \| 2^+ \rangle,$$

as will be further explained later.

The magnetic-dipole and electric-quadrupole transition probabilities were calculated by evaluating the operators $\boldsymbol{\mu}$ and $\mathbf{Q}_e$, defined as

$$\boldsymbol{\mu} = \mu_0 \left[g_c \mathbf{J}_c^{(1)} + g_l \mathbf{l}_n^{(1)} + g_s \mathbf{s}_n^{(1)} \right],$$
$$\mathbf{Q}_e = \sqrt{\frac{16\pi}{5}} \left\{ e_c \mathbf{Q}_c^{(2)} + e_n \mathbf{Q}_n^{(2)} \right\},$$

where μ_0 is the nuclear magneton, g_l and g_s are the orbital and spin neutron single-particle gyromagnetic factors, g_c is that of the core, and e_c and e_n are the core and particle effective charges, respectively. The usual (for this model) effective values of $g_s = 0.6 g_{s(\text{free})}$, $g_c = Z/A$, and $e_n = 1e$ were adopted for the calculation (this choice was further evaluated by comparing the calculated ground-state static dipole and quadrupole moments, as will be seen in Table III). As for e_c, since it reflects in a sense the unknown dynamics of the core, its value is taken from the experiment by using its relation to χ_1 and the reduced transition probability of the core:

$$e_c^2 = \frac{B(E2\downarrow; \text{core})}{|\langle 0^+ \| \mathbf{Q}_c^{(2)} \| 2^+ \rangle|^2},$$

where $B(E2\downarrow;\text{core})$ is taken from the experimental data. In this way, the calculated level pattern is related to the electric-quadrupole properties and to the actual core dynamics which enters via the use of the experimental $B(E2)$ value.

We note for the sake of completeness that, to limit the number of parameters to a strict minimum, and contrary to Ref. [39], we excluded the excitations with the 3^- core state in the calculations. Moreover, existence of octupole excitations in the ^{84}Se core is not as well established as it is in the ^{88}Sr and ^{86}Kr cores. The main drawback is that the negative-parity states are not described in our approach. Similarly, contrary to Ref. [39], the core 2_1^+ energy was not allowed to vary in the fitting procedure. In these conditions, agreement between

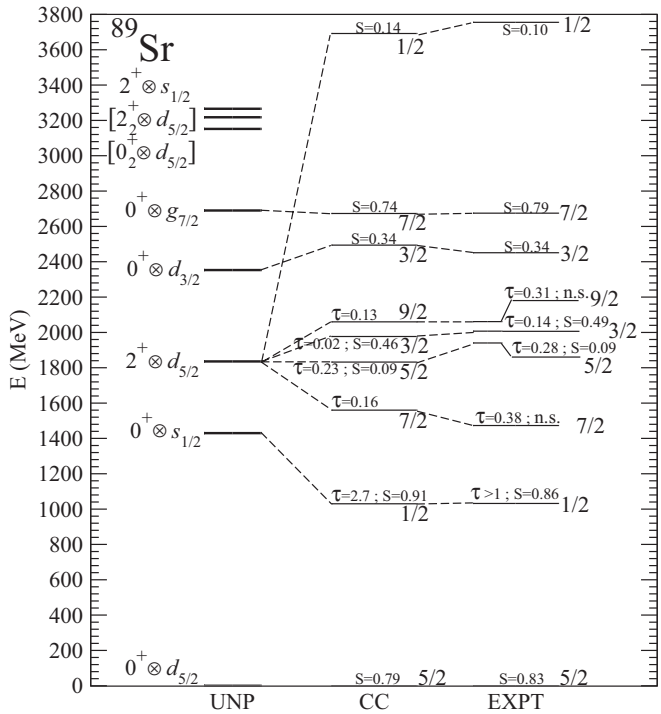

FIG. 13. Comparison between the core-coupling (middle column "CC") and experimental (right column "EXPT") level schemes for ^{89}Sr. The unperturbed energy of the core-coupled configurations are represented on the left column ("UNP"). Configurations expected in this energy region but not included in the calculations are with square brackets. Spectroscopic factors S are written close to their associate levels, as well as some of the relevant lifetime values, τ, given in ps. The experimental values for S and τ were taken from Refs. [42] and [43], respectively (see also the full $A = 89$ evaluation [41]).

theory and experiment cannot be expected in spectral regions located much above the core one-phonon excitation energy.

Several experimental lifetime and spectroscopic factor values are available for ^{89}Sr [41], which was used as a reference nucleus. The comparison between theory and experiment is provided in Fig. 13. Overall, the agreement is far better than simply qualitative, as was already the case in Ref. [39], although in that work no information was provided on lifetimes. Compared with Ref. [39], we obtain slight improvements for the overall level-scheme pattern (particularly for the $9/2^+_1$ state and the high-lying weakly stripping $1/2^+$ states) but very similar spectroscopic factors. In addition, we provide information on the expected lifetimes for these states. These are in agreement with the experimental lifetimes within at maximum a factor two. As mentioned earlier, to further verify the choice of the effective charges, the ground-state static magnetic-dipole and electric-quadrupole moments for ^{89}Sr, ^{87}Kr, and ^{85}Se were calculated and compared with the experimental values when available (Table III). The $7/2^+_1$ state wave function is dominated by the $2^+ \otimes 2d_{5/2}$ configuration at 98%. We note that, for the transition connecting this state and the ground state, we obtain a $\delta(E2/M1)$ mixing coefficient which is slightly higher, with $\delta = 0.93$, than the experimental value of $\delta = 0.75(7)$ [43]. This is probably

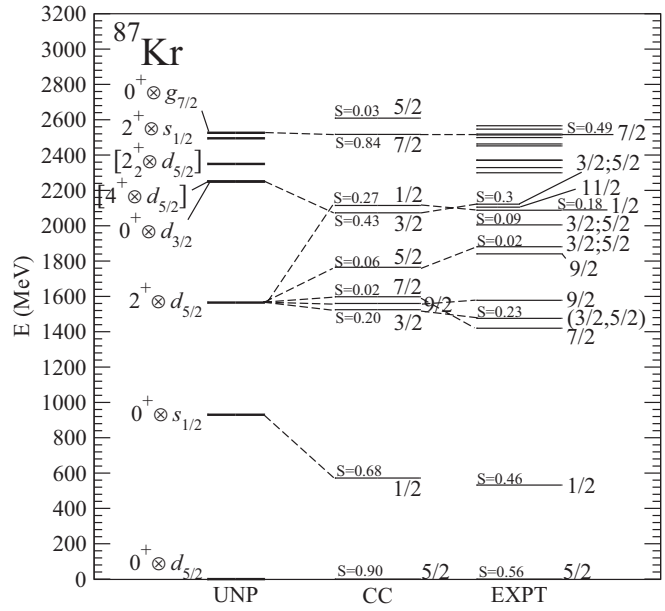

FIG. 14. Same as Fig. 13 but for ^{87}Kr (experimental S values are from Ref. [17]).

related to the fact that the $0^+ \otimes 1g_{7/2}$ component of the $7/2^+_1$ state is slightly underestimated. However, the order of magnitude is definitely correct, which shows that, although slightly overestimated, the $E2/M1$ mixing of the transition depopulating the (mainly $2^+ \otimes 2d_{5/2}$ core-coupled) $7/2^+_1$ state to the (mainly $0^+ \otimes 2d_{5/2}$) $5/2^+$ ground state is well under control in our approach.

Following these encouraging results, calculations were pursued also for the ^{87}Kr and ^{85}Se cases, and the results are shown in Figs. 14 and 15. The modifications of the $5/2^+_{gs}$

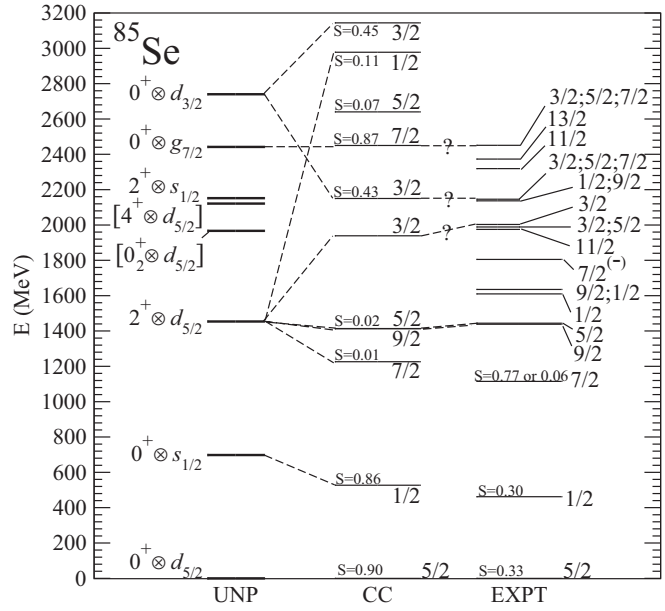

FIG. 15. Same as Fig. 13 but for ^{85}Se (experimental S values are from Ref. [11]).

TABLE IV. Experimental and core-coupling-model results for the energy and lifetime values of the $7/2_1^+$ state in the three $N = 51$ isotones ^{89}Sr, ^{87}Kr, and ^{85}Se. For the lifetime, both results obtained directly from the fit parameters, which correspond to a major wave function $2^+ \otimes 2d_{5/2}$ component, and in the "inverted" case ($0^+ \otimes 1g_{7/2}$) are given (see text for more explanations).

	Experiment		Theory		
	E (keV)	τ (ps)	E (keV)	τ (ps)	
				$2^+ \otimes 2d_{5/2}$	$0^+ \otimes 1g_{7/2}$
^{89}Sr	1473	0.38(14) [43]	1559	0.16	14.9
^{87}Kr	1420	$0.4^{+1.6}_{-0.4}$	1598	0.19	23.2
^{85}Se	1115	3(2)	1226	0.42	79.5

and $7/2_1^+$ wave functions from ^{89}Sr to ^{85}Se are marginal. The small changes of the $7/2_1^+$ lifetimes are then mainly due to changes of the $7/2_1^+$ excitation energies from one nucleus to the other. The lifetime results for the three nuclei are summarized in Table IV. To get a quantitative estimate of the lifetime value in the case of the $7/2_1^+$ state with a very large spectroscopic factor (as would be expected for ^{85}Se according to Ref. [11]), the $7/2_1^+ \rightarrow 5/2_{gs}^+$ transition properties were calculated by artificially interchanging the $2^+ \otimes 2d_{5/2}$ and $0^+ \otimes 1g_{7/2}$ amplitudes in the $7/2_1^+$ wave function. As can be seen in Table IV, this inevitably leads to an increase by about two orders of magnitudes in the lifetime values (values in the Weisskopf range). In this "inverted" case, $\delta(E2/M1)$ mixing ratios are reduced to values of the order of $\approx$0.2 for the three $N = 51$ isotones considered. This shows that, while being strongly retarded, the $7/2_1^+ \rightarrow 5/2_{gs}^+$ transition also becomes essentially $M1$ in nature.

In conclusion, according to these core-coupling calculations, the $7/2_1^+$ states lifetimes obtained in our experiment are only compatible with a situation where the $2^+ \otimes 2d_{5/2}$ configuration dominates the $7/2_1^+$ wave functions with a minor ($\lesssim$10%) $0^+ \otimes 1g_{7/2}$ component.

Since this would be, in a sense, a phenomenology-driven theory-based conclusion, we additionally compare these results with those from a different, fully microscopic approach in the following section. This will be the occasion, in addition, to quantify the influence of the couplings to higher-energy core states (neglected in these core-coupling calculations) on the low-energy structure.

B. Shell-model approach

The shell-model calculations performed here, using the full valence space outside the ^{78}Ni core, are a continuation of the work initiated in Ref. [3]. These calculations provide a correct description of the collectivity evolution close to ^{78}Ni and are consistent with results obtained by beyond-mean-field techniques [5]. They were also shown to be successful in describing the structure of the light $N = 51$ isotone ^{83}Ge [4]. The present calculations include some optimizations for the $N = 50$ region performed in the light of recent experimental results; see Refs. [8,45]. In the calculations of magnetic transitions we use the quenching factor of 0.7 for the spin part while $0.7e$ polarization charge is used for the electric operator, as done previously in this region, e.g., in Ref. [3]. As can be seen from Table III, both magnetic and electric moments of the ground state calculated this way are in fair agreement with experiment and with the core-coupling-model calculations. The shell model predicts quite pure structures of the $5/2^+$ ground states in all three nuclei: 87%, 85%, and 84% of the $0^+ \otimes 2d_{5/2}$ configuration in ^{89}Sr, ^{87}Kr, and ^{85}Se, respectively.

TABLE V. Shell-model results for the energies and lifetimes of selected 2^+ core-coupled states in ^{89}Sr, ^{87}Kr, and ^{85}Se. The main configurations entering into the wave function are given in percentage. In bold is given information for the $7/2_1^+$ states of main interest here.

	J^π	E (keV)	τ (ps)	Configurations	
				$2^+ \otimes 2d_{5/2}$	$4^+ \otimes 2d_{5/2}$
^{89}Sr	**$7/2_1^+$**	**1488**	**0.16**	**95%**	
	$3/2^+$	1864	0.02	61%	
	$5/2_2^+$	1888	0.10	83%	
	$9/2^+$	2013	0.12	94%	
^{87}Kr	$3/2^+$	1401	0.03	78%	
	$9/2^+$	1424	0.74	84%	12%
	$1/2_2^+$	1543	1.5	63%	
	$7/2_1^+$	**1673**	**0.17**	**51%**	**41%**
^{85}Se	$3/2^+$	1227	0.05	79%	
	$9/2^+$	1234	0.96	84%	11%
	$1/2_2^+$	1461	4.3	57%	
	$7/2_1^+$	**1660**	**0.13**	**61%**	**28%**

In Table V we summarize the shell-model results for the lowest states belonging to the 2^+ core-coupled multiplet in the case of ^{89}Sr, ^{87}Kr, and ^{85}Se (we select the first state of each spin below $\sim$2 MeV, containing at least 50% of the $2^+ \otimes 2d_{5/2}$ component in the wave functions). Shell-model lifetimes are obtained by taking into account $E2$ and $M1$ transitions to all calculated final states. As one can see, in ^{89}Sr the order of the shell-model states in the multiplet and their lifetimes are very close to those from the core-coupling model with a pure $2^+ \otimes 2d_{5/2}$ configuration, which clearly dominates the calculated shell-model wave functions. The lowest $7/2^+$ state is thus the core-coupled one, while the second $7/2^+$ state, calculated at 2.4 MeV, contains 79% of the $0^+ \otimes 0g_{7/2}$ configuration. As for the $7/2_1^+$ states of ^{87}Kr and ^{85}Se, the main component of the wave function corresponds to a $2^+ \otimes 2d_{5/2}$ configuration, consistent with the core-coupling approach, but one notes a non-negligible contribution from the $4^+ \otimes 2d_{5/2}$ configuration. However, contrary to the core-coupling results, the $7/2_1^+$ state appears above the $3/2^+$ and $9/2^+$ members of the multiplet. For that reason, the shell-model $7/2_1^+$ state also decays to these two states. The calculated lifetime in ^{87}Kr is, however, in good agreement with that obtained by the core-coupling calculation. In ^{85}Se the agreement is less impressive but the order of magnitude of the two lifetimes is the same. One should note that the shell-model calculations overestimate considerably the $7/2_1^+$ energy. If the experimental value (1115 keV) is used instead in the lifetime calculation,

the value of 0.56 ps is obtained, in a closer agreement with the core-coupled calculation. This shows that the omission of the higher core-coupled states is of little importance for the lifetime evaluation of the states of interest here. The $7/2_1^+ \rightarrow 5/2_{gs}^+$ transition is slightly dominated by the $M1$ component [$\delta^2(E2/M1) = 0.84; 0.57$ for ^{87}Kr;^{85}Se] in the shell-model case while it is the opposite [$\delta^2(E2/M1) = 1.05; 1.14$ for ^{87}Kr;^{85}Se] in the core-coupling case. Despite these slight differences, it can be concluded that these shell-model calculations lead to lifetime values for the $7/2_1^+$ state well within the range we have experimentally determined, and to a $7/2_1^+$ wave function dominated by the core-coupled $2^+ \otimes 2d_{5/2}$ configuration. This significantly strengthens the conclusion drawn previously from a different, much more phenomenological approach.

VI. CONCLUSION

Lifetime measurements of excited states were performed for the first time in the light $N = 51$ odd isotones ^{87}Kr and ^{85}Se by using the Cologne plunger device coupled to the AGATA Demonstrator for γ detection and the PRISMA spectrometer for particle identification at the LNL Tandem-ALPI facility. Shifted-to-unshifted ratios were measured for ten transitions in ^{87}Kr and two in ^{85}Se from which the intrinsic lifetimes of seven excited states in ^{87}Kr and upper limits for the $7/2_1^+$ and $9/2_1^+$ excited states in ^{85}Se could be determined.

Our main objective was to complement with lifetime information the very scarce direct neutron exchange reaction data on the $7/2_1^+$ state in ^{85}Se to assess whether it carries a significant fraction of the $\nu 1g_{7/2}$ single-particle strength. It was motivated by the idea that the ESPE evolution towards $Z = 28$ of the $\nu 1g_{7/2}$ orbital should be dominated by the tensor part of the residual proton-neutron interaction because it is characterized by a large orbital angular momentum, $\ell = 4$. According to the tensor mechanism, larger and larger $\nu 1g_{7/2}$ components should appear in the $7/2_1^+$ wave functions of the $N = 51$ odd-isotones when approaching ^{79}Ni.

The short lifetime ($\tau = 0.4^{+1.6}_{-0.4}$ ps) which we obtain for the ($7/2_1^+$) state in ^{87}Kr is characteristic of the core-coupled $2^+ \otimes \nu 2d_{5/2}$ (collective in a sense) description of this state in both shell-model and core-coupling calculations. It is also consistent with the fact that this state is not populated by direct neutron exchange reactions. The ^{87}Kr case provides then a clear proof of principle for the alternative, lifetime-based method proposed here.

From the upper limit of 3(2) ps for the $7/2_1^+$ state lifetime that we could determine in the case of ^{85}Se (and its comparison with both core-coupling and shell-model calculations) it can also be concluded that this level is much too short lived to contain a significant fraction of the $\nu 1g_{7/2}$ strength. This result is not compatible with the results of the—nevertheless pioneering and challenging—work of Ref. [11], where this $7/2_1^+$ state was populated in the reaction ^{2}H(^{84}Se, p)^{85}Se with a spectroscopic factor $S = 0.77 \pm 0.27$ in case of an $\ell = 4$ wave.

One would have expected qualitatively that the same tensor mechanism which seems to be responsible for the clear $\nu 1g_{7/2}$ ESPE down sloping towards ^{101}Sn (and the quasi $\nu 2d_{5/2}$-$\nu 1g_{7/2}$ degeneracy dominating the low-energy structure in the ^{100}Sn region) would also lead to a mirror situation in the ^{78}Ni region. From our results it seems that the situation is somewhat more involved and it remains to be verified theoretically how other terms of the nucleon-nucleon interaction contribute to the shell evolution in this region. On the experimental side, it remains to be verified whether larger $\nu 1g_{7/2}$ contributions appear in the $7/2_1^+$ states of the lighter $N = 51$ isotones ^{83}Ge and ^{81}Zn and ultimately where the main $\nu 1g_{7/2}$ single-particle strength is located in energy. The alternative experimental strategy that we have developed and exposed in this paper, based on lifetime measurements, could be of some help in these future endeavors.

ACKNOWLEDGMENTS

We are grateful to the staff of the Tandem-ALPI accelerator for the smooth running conditions during this experiment. This work was partially supported by the European Union Seventh Framework Program FP7/2007-2013 under Grant Agreement No. 262010 ENSAR and by the German Research Foundation (DPG) under Contract No. DE 1516/3-1. J.L. thanks the Bonn–Cologne Graduate School of Physics and Astronomy (BCGS) for financial support.

[1] D. K. Sharp, B. P. Kay, J. S. Thomas, S. J. Freeman, J. P. Schiffer, B. B. Back, S. Bedoor, T. Bloxham, J. A. Clark, C. M. Deibel, C. R. Hoffman, A. M. Howard, J. C. Lighthall, S. T. Marley, A. J. Mitchell, T. Otsuka, P. D. Parker, K. E. Rehm, D. V. Shetty, and A. H. Wuosmaa, Phys. Rev. C **87**, 014312 (2013).

[2] J. Duflo and A. P. Zuker, Phys. Rev. C **59**, R2347 (1999).

[3] K. Sieja, F. Nowacki, K. Langanke, and G. Martinez-Pinedo, Phys. Rev. C **79**, 064310 (2009).

[4] K. Kolos, D. Verney, F. Ibrahim, F. Le Blanc, S. Franchoo, K. Sieja, F. Nowacki, C. Bonnin, M. C. Mhamed, P. V. Cuong, F. Didierjean, G. Duchêne, S. Essabaa, G. Germogli, L. H. Khiem, C. Lau, I. Matea, M. Niikura, B. Roussière, I. Stefan, D. Testov, and J.-C. Thomas, Phys. Rev. C **88**, 047301 (2013).

[5] K. Sieja, T. R. Rodríguez, K. Kolos, and D. Verney, Phys. Rev. C **88**, 034327 (2013).

[6] A. Korgul, K. P. Rykaczewski, R. Grzywacz, H. Sliwinska, J. C. Batchelder, C. Bingham, I. N. Borzov, N. Brewer, L. Cartegni, A. Fijalkowska, C. J. Gross, J. H. Hamilton, C. Jost, M. Karny, W. Krolas, S. Liu, C. Mazzocchi, M. Madurga, A. J. Mendez, K. Miernik, D. Miller, S. Padgett, S. Paulauskas, D. Shapira, D. Stracener, K. Sieja, J. A. Winger, M. Wolinska-Cichocka, and E. F. Zganjar, Phys. Rev. C **88**, 044330 (2013).

[7] M. Czerwiński, T. Rząca-Urban, K. Sieja, H. Sliwinska, W. Urban, A. G. Smith, J. F. Smith, G. S. Simpson, I. Ahmad, J. P. Greene, and T. Materna, Phys. Rev. C **88**, 044314 (2013).

[8] T. Materna, W. Urban, K. Sieja, U. Köster, H. Faust, M. Czerwiński, T. Rząca-Urban, C. Bernards, C. Fransen, J. Jolie, J.-M. Regis, T. Thomas, and N. Warr, Phys. Rev. C **92**, 034305 (2015).

[9] O. Sorlin and M.-G. Porquet, Prog. Part. Nucl. Phys. **61**, 602 (2008).

[10] J. S. Thomas, D. W. Bardayan, J. C. Blackmon, J. A. Cizewski, U. Greife, C. J. Gross, M. S. Johnson, K. L. Jones, R. L. Kozub, J. F. Liang, R. J. Livesay, Z. Ma, B. H. Moazen, C. D. Nesaraja, D. Shapira, and M. S. Smith, Phys. Rev. C **71**, 021302(R) (2005).

[11] J. S. Thomas, G. Arbanas, D. W. Bardayan, J. C. Blackmon, J. A. Cizewski, D. J. Dean, R. P. Fitzgerald, U. Greife, C. J. Gross, M. S. Johnson, K. L. Jones, R. L. Kozub, J. F. Liang, R. J. Livesay, Z. Ma, B. H. Moazen, C. D. Nesaraja, D. Shapira, M. S. Smith, and D. W. Visser, Phys. Rev. C **76**, 044302 (2007).

[12] D. Verney, F. Ibrahim, C. Bourgeois, S. Essabaa, S. Galés, L. Gaudefroy, D. Guillemaud-Mueller, F. Hammache, C. Lau, F. Le Blanc, A. C. Mueller, O. Perru, F. Pougheon, B. Roussière, J. Sauvage, and O. Sorlin, Phys. Rev. C **76**, 054312 (2007).

[13] S. Padgett, M. Madurga, R. Grzywacz, I. G. Darby, S. N. Liddick, S. V. Paulauskas, L. Cartegni, C. R. Bingham, C. J. Gross, K. Rykaczewski, D. Shapira, D. W. Stracener, A. J. Mendez, II, J. A. Winger, S. V. Ilyushkin, A. Korgul, W. Królas, E. Zganjar, C. Mazzocchi, S. Liu, J. H. Hamilton, J. C. Batchelder, and M. M. Rajabali, Phys. Rev. C **82**, 064314 (2010).

[14] V. Paziy *et al.*, JPS Conf. Proc. **6**, 030009 (2015), Proc. Conf. Advances in Radioactive Isotope Science, ARIS2014, Tokyo, June 2014 (Physical Society of Japan, 2015).

[15] T. Otsuka, T. Suzuki, R. Fujimoto, H. Grawe, and Y. Akaishi, Phys. Rev. Lett. **95**, 232502 (2005).

[16] T. Otsuka, T. Suzuki, M. Honma, Y. Utsuno, N. Tsunoda, K. Tsukiyama, and M. Hjorth-Jensen, Phys. Rev. Lett. **104**, 012501 (2010).

[17] K. Haravu, C. L. Hollas, P. J. Riley, and W. R. Coker, Phys. Rev. C **1**, 938 (1970).

[18] G. de Angelis, Nucl. Phys. A **787**, 74 (2007).

[19] M.-G. Porquet *et al.*, Eur. Phys. J. A **39**, 295 (2009).

[20] J. Omtvedt, B. Fogelberg, and P. Hoff, Z. Phys. A: Hadrons Nucl. **339**, 349 (1991).

[21] J. Kurpeta, W. Urban, T. Materna, H. Faust, U. Köster, J. Rissanen, T. Rząca-Urban, C. Mazzocchi, A. G. Smith, J. F. Smith, J. P. Greene, and I. Ahmad, Phys. Rev. C **85**, 027302 (2012).

[22] S. Szilner, C. A. Ur, L. Corradi, N. Marginean, G. Pollarolo, A. M. Stefanini, S. Beghini, B. R. Behera, E. Fioretto, A. Gadea, B. Guiot, A. Latina, P. Mason, G. Montagnoli, F. Scarlassara, M. Trotta, G. de Angelis, F. Della Vedova, E. Farnea, F. Haas, S. Lenzi, S. Lunardi, R. Marginean, R. Menegazzo, D. R. Napoli, M. Nespolo, I. V. Pokrovsky, F. Recchia, M. Romoli, M. D. Salsac, N. Soic, and J. J. Valiente-Dobon, Phys. Rev. C **76**, 024604 (2007).

[23] L. Corradi *et al.*, Nucl. Instrum. Methods Phys. Res., Sect. B **317**, Part B, 743 (2013).

[24] S. Akkoyun *et al.*, Nucl. Instrum. Methods Phys. Res., Sect. A **668**, 26 (2012).

[25] A. Gadea *et al.*, Nucl. Instrum. Methods Phys. Res., Sect. A **654**, 88 (2011).

[26] R. Venturelli and D. Bazzacco, LNL Annual Report 2004, LNL-INFN, Legnaro, Italy (2005), p. 220.

[27] F. Recchia *et al.*, Nucl. Instrum. Methods Phys. Res., Sect. A **604**, 555 (2009).

[28] P.-A. Söderström *et al.*, Nucl. Instrum. Methods Phys. Res., Sect. A **638**, 96 (2011).

[29] A. Lopez-Martens, K. Hauschild, A. Korichi, J. Roccaz, and J.-P. Thibaud, Nucl. Instrum. Methods Phys. Res., Sect. A **533**, 454 (2004).

[30] T. Alexander and A. Bell, Nucl. Instrum. Methods **81**, 22 (1970).

[31] A. Dewald, O. Möller, and P. Petkov, Prog. Part. Nucl. Phys. **67**, 786 (2012).

[32] J. Litzinger *et al.*, Phys. Rev. C **92**, 064322 (2015).

[33] http://lise.nscl.msu.edu.

[34] A. Dewald, S. Harissopulos, and P. von Brentano, Z. Phys. A At. Nucl. **334**, 163 (1989).

[35] http://root.cern.ch.

[36] M.-G. Porquet *et al.*, Eur. Phys. J. A **28**, 153 (2006).

[37] O. Perru *et al.*, Eur. Phys. J. A **28**, 307 (2006).

[38] A. Etilé, D. Verney, N. N. Arsenyev, J. Bettane, I. N. Borzov, M. C. Mhamed, P. V. Cuong, C. Delafosse, F. Didierjean, C. Gaulard, N. Van Giai, A. Goasduff, F. Ibrahim, K. Kolos, C. Lau, M. Niikura, S. Roccia, A. P. Severyukhin, D. Testov, S. Tusseau-Nenez, and V. V. Voronov, Phys. Rev. C **91**, 064317 (2015).

[39] P. H. Hoffmann-Pinther and J. L. Adams, Nucl. Phys. A **229**, 365 (1974).

[40] V. K. Thankappan and W. W. True, Phys. Rev. **137**, B793 (1965).

[41] B. Singh, Nucl. Data Sheets **114**, 1 (2013).

[42] T. P. Cleary, Nucl. Phys. A **301**, 317 (1978).

[43] E. Wallander *et al.*, Nucl. Phys. A **361**, 387 (1981).

[44] T. Johnson and W. Kulp, Nucl. Data Sheets **129**, 1 (2015).

[45] M. Czerwiński, T. Rząca-Urban, W. Urban, P. Bączyk, K. Sieja, B. M. Nyakó, J. Timár, I. Kuti, T. G. Tornyi, L. Atanasova, A. Blanc, M. Jentschel, P. Mutti, U. Köster, T. Soldner, G. de France, G. S. Simpson, and C. A. Ur, Phys. Rev. C **92**, 014328 (2015).